



On the emergence of 3D printable Engineered, Strain Hardening Cementitious Composites (ECC/SHCC)



Victor C. Li^{a,*}, Freek P. Bos^b, Kequan Yu^a, Wes McGee^c, Tsz Yan Ng^c, Stefan Chaves Figueiredo^b, Karsten Nefs^b, Viktor Mechtcherine^d, Venkatesh Naidu Nerella^d, Jinlong Pan^e, Gideon P.A.G. van Zijl^f, P. Jacques Kruger^f

^a Department of Civil and Environmental Engineering, University of Michigan, Ann Arbor, USA

^b Department of the Built Environment, Eindhoven University of Technology, the Netherlands

^c Taubman College of Architecture and Urban Planning, University of Michigan, Ann Arbor, USA

^d Institute of Construction Materials, TU Dresden, Dresden, Germany

^e Department of Civil Engineering, Southeast University, Nanjing, China

^f Division of Structural Engineering and Civil Engineering Informatics, Stellenbosch University, South Africa

ARTICLE INFO

Keywords:

3D concrete printing

ECC

SHCC

Ductility

Printability

ABSTRACT

While interest in 3D printing of concrete (3DCP) and structures has been growing, a major obstacle for implementation of 3DP construction method is the need for steel reinforcement and the challenges this presents to the 3DP process. Engineered Cementitious Composites (ECC), also known as Strain-hardening Cement-based Composites (SHCC), hold promise to attain structural integrity, durability, reliability and robustness without steel reinforcement. This article surveys the state of the art on 3DP research with ECC and suggests needed research to direct future development. Research in Asia, Europe and the United States has demonstrated printability and buildability of 3DP-ECC that exhibits characteristic tensile ductility of cast ECC. Nonetheless, a number of outstanding research areas are identified, including those associated with more sustainable mix-design, rheology control, microstructure, filament/filament interface weakness, and long-term durability. Resolution of these challenges will better position the research community to addressing full scale construction, print speed, and print quality.

1. Introduction

Engineered Cementitious Composites (ECC) (also known as Strain-hardening Cement-based Composites, SHCC) was developed over two decades ago by the first author of this article, in response to the need to overcome concrete's brittleness [1,2]. While significant advancements in concrete have taken place ever since Portland Cement was invented about two hundred years ago, accompanied by an almost continuous increase in compressive strength, concrete itself has remained a quasi-brittle material, even when fiber was used as dispersed reinforcement. This changed with the invention of ECC, the first cement-based material which yielded tensile ductility at reasonably low fiber contents of 1 to 2% by volume. Fig. 1 shows the high ductility of ECC in a flexural bending experiment, in contrast to brittle fracture of a similarly loaded high strength concrete slab.

The brittleness of concrete has imposed limits on both resilience and durability of concrete structures, even when reinforced with steel. ECC

offers opportunities to overcome these limitations, and further supports infrastructure sustainability through the reduction of operations and maintenance needs.

ECC is emerging in full scale structures, including bridges [3,4], road pavements [106] and high rise buildings [5]. It has also found use in repair and retrofit of existing structures [1,6,7]. In these applications, ECC offers values in extended service life, improved functions such as leak-proofing and energy absorption, and in reduced installed cost. These values are generally derived from the high tensile ductility of ECC (several hundred times that of normal concrete) and from the intrinsically tight crack width (below 100 μm).

Considering these unique properties and advantages, it is not surprising that ECC is attracting attention as a material for innovative concrete manufacturing methods, such as extrusion-based 3D concrete printing (3DCP). 3DCP is the most common technique among a group of recently introduced digital and additive manufacturing methods for concrete and cementitious materials, of which other technologies

* Corresponding author.

E-mail address: vcli@umich.edu (V.C. Li).

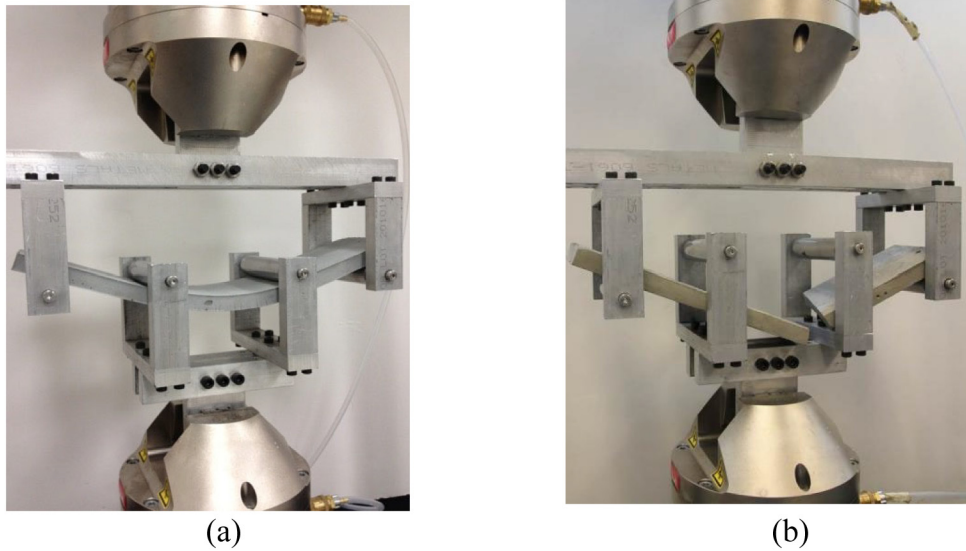


Fig. 1. (a) Ductile ECC under bending load, in contrast to (b) brittle fracture of high strength concrete [1].

include binder-jetting, robotically controlled concrete spraying, and adaptive sliding formwork [8]. Although attractive for its geometric freedom and reduced use of material and labor, currently, the 3DCP process is incompatible with conventional reinforcement methods that may limit the potential advantages of 3DCP. Therefore, a range of new reinforcement concepts is being explored [9–11]. A distinctive feature of many 3D concrete printed structural elements, in comparison to conventional cast concrete, is their slenderness, which is a consequence of architectural design preferences and structural optimization. This renders printed objects particularly prone to damage (often accidental) due to local loads and impacts during construction and in use. In conventional concrete, the massive nature in combination with steel reinforcement makes this inconsequential. In 3DCP, the robustness of printed objects becomes much more critical.

ECC potentially provides an attractive solution to these issues concerning non-compatibility of 3D printing (3DP) with steel reinforcement and possible lack of structural robustness. The self-reinforcing characteristic [12,13] inherent in the material obviate the need for additional processing steps and significantly decreases the sensitivity to local failures, like chipping. Since ECCs are particularly well-equipped to absorb impact energy [14–16], they are very suitable for high-slenderness printed structures. However, for a variety of reasons, the development and application of printable ECC (3DP-ECC) is not self-evident. The purpose of this paper is to review the potential and challenges of 3DP-ECC.

With respect to fresh property requirements, the conflicting demands between pumpability and buildability is amplified by the relatively high fiber content (~2% by volume) and small fiber diameter (typically below 50 μm) essential for retaining the strain-hardening property of ECC. The extrusion-based 3DP process should help in fiber alignment in the direction of the laid-down filament, leading to a more-or-less 1D-2D orientation that is advantageous to in-plane mechanical property. The layer-by-layer build-up process, however, may result in weaker interface with limited fiber bridging across this interface. This potential weakness needs to be characterized and effective approaches to toughening the layer-to-layer interface need to be developed.

This review paper covers the work conducted in several groups focusing on 3DP-ECC research in Asia [17,18], Europe [19,20] and in the United States [12,21]. Research in 3DP-ECC remains at any early stage but is expected to expand globally at a rapid pace.

2. Theoretical considerations

2.1. Principles and performance of ECC

The mechanical performance of ECC is characterized by its uniquely high tensile ductility and pseudo strain hardening behavior, which occurs when fibers enable the development of multiple cracks in a brittle matrix under increasing stress and strain (hereafter simply referred to as ‘strain hardening’ for brevity). The compressive strength of ECC can be tailored between low (several MPa, for fire-resistant sprayable ECC [22]) to high (over 200 MPa, for structural applications and strengthening [23–26]). Fig. 2 shows the tensile stress-strain curve of a moderate and a high strength ECC. The tensile stress-strain curve of an ultra-high performance concrete (UHPC) [27] is also shown for comparison. It is seen that the compressive strength of ECC can match that of UHPC, but its tensile ductility is at least one order of magnitude higher.

In designing ECC, the basic principle emphasizes synergies between fiber, matrix, and fiber/matrix interface. The theoretical design basis is described in detailed in [1]. A brief summary of the two criteria is given here:

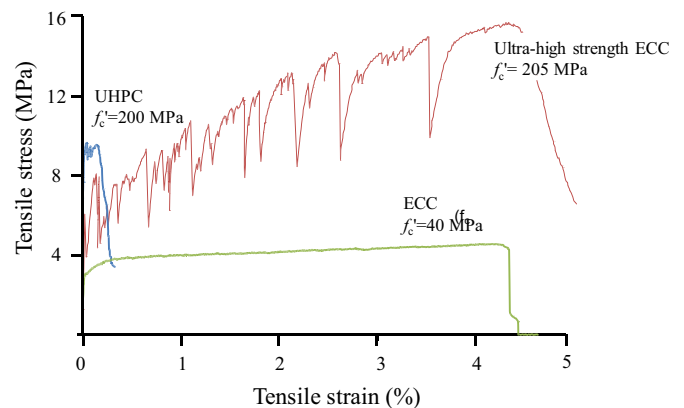


Fig. 2. Tensile stress-strain curves of normal strength and high strength ECC, and UHPC. Both ECCs have tensile strain capacity several hundred times that of normal concrete [1]. Data were determined from uniaxial tensile tests on coupon specimens of 305 mm \times 76 mm \times 12.7 mm, with a gage length of 101 mm, following the JSCE (Japan Society of Civil Engineers) testing protocol [28].

The strength criterion requires that the tensile stress at first crack σ_{fc} must be below the fiber bridging strength σ_0 . Violating this condition leads to the initiation of the first crack that breaks or pulls out all the fibers crossing that crack, resulting in a tension-softening response.

$$\sigma_{fc} < \sigma_0 \quad (1)$$

If Eq. (1) is satisfied, crack propagation follows after initiation, during which the balance of work energy $\sigma_0 \delta_0$ and energy consumed by breaking down crack tip material J_{tip} as well as energy absorbed in the near-crack-tip fiber bridging zone (represented by the integral term in Eq. (2)) requires that

$$\sigma_0 \delta_0 - \int_0^{\delta_0} \sigma(\delta) d\delta \equiv J'_b \geq J_{tip} \quad (2)$$

where δ_0 is the steady state opening of the crack flank. $\sigma(\delta)$ is the crack bridging traction as a function of crack opening δ given by

$$\sigma(\delta) = \frac{V_f}{A_f} \int_{\phi_0}^{\phi_1} \int_{z=0}^{(L_f/2) \cos \phi} P(\delta, L_e) g(\phi) p(\phi) p(z) dz d\phi \quad (3)$$

In Eq. (3), V_f , A_f , and L_f are fiber volume content, fiber cross sectional area, and fiber length. The fiber embedment length L_e is defined by the fiber length, centroidal distance z of fiber from the crack plane, and fiber orientation angle (relative to the normal of the crack plane) ϕ . L_e and ϕ are treated as random variables describing the probability of fiber location $p(z)$ and fiber orientation $p(\phi)$. ϕ_0 and ϕ_1 limits the range of orientation. For example, if fibers are restricted to within zero degree and 45° , then $\phi_0 = 0$ and $\phi_1 = 45^\circ$. Naturally, the narrower the orientation range, the more aligned the fibers are, as could be induced by the extrusion process of 3DP (also see Section 4.4).

$P(\delta, L_e)$ in Eq. (3) represents the single fiber force resistance at fiber end displacement of δ in the case of single-sided pull out. $g(\phi)$ represents the bridging force modification caused by inclined fibers from that of straight pull-out. Eq. (3) is used inside the integral in Eq. (2).

Eqs. (1) and (2) dictate fiber, matrix, and interface properties that must be synergized to achieve tensile strain-hardening. These criteria are used in systematic design of ECCs.

Physically, strong fiber bridging is desirable – and is associated with high fiber content and fiber strength. However, excessively strong mortar matrix via either high toughness J_{ip} or small defect size, may lead to catastrophic fracture failure in the form of tension-softening rather than strain-hardening once a crack is initiated. The most important balancing act occurs in the fiber/matrix interfacial bond measured in terms of interface toughness and friction. In general, a lower chemical bond is desirable to allow interfacial slippage to initiate, but a higher frictional bond is desirable to dissipate energy during sliding. Note that interfacial slippage does not necessarily mean a loss of chemical bond over the entire length of the fiber, but rather stretching of the fiber over the de-bonded segment of fiber. Furthermore, fiber slippage often results in a particular type of damage, a “locking front”, somewhere on the fiber's embedded length, which leads to a rise in force in the post-de-bonding regime [29]. It can be seen, therefore, that the design principle of ECC is distinctively different from that for UHPC, which usually emphasizes dense packing of particles in the binder phase of the composite.

The 3DP process is expected to have impacts on all three phases of the ECC composite. Specifically, fibers may have preferred orientation along the print path, resulting in higher bridging capacity for cracks normal to the print filament. Further, the matrix defect population size distribution as well as the fiber/matrix interfaces may be modified by the extruder end-effector if a compression load is exerted on the filament during printing.

Eq. (3) can also be used to study the effect of fiber orientation range on the stress vs crack-opening relationship. It can be used to compute the maximum fiber bridging stress corresponding to the peak ultimate

tensile strength σ_0 , as well as the complementary energy J'_b . The effects of 3DP process on ECC properties are further discussed in Section 4.

The structural performance of ECC has been summarized in [1], although most structural response studies have been conducted on steel reinforced ECC. In case of quasi-static loading, the interaction of ECC with steel reinforcement further facilitates multiple cracking and enhances tensile strain capacity during the stage of elastic steel deformation [30]. Several studies [31,32] illustrated that the amount of shear reinforcement can be minimized or eliminated altogether, all the while, maintaining structural performance in fully reversed cyclic loading. In side-by-side comparative studies, Kesner & Billington [33] demonstrated that structural capacity is actually higher in shear panels built with R/ECC (steel reinforced ECC) compared to that of R/C using concrete with higher compressive strength, demonstrating the importance of ECC tensile ductility (as opposed to compressive strength) to structural capacity. Of particular relevance to 3DP without steel reinforcement, a study by Yu et al. [13] demonstrated that a two-story frame building built with a high strength ECC performed well under a shake table test – verifying that ECC may serve structural performance needs with limited or no conventional steel reinforcement.

2.2. Extrusion-based 3DCP

In 3DCP, a filament of cementitious mortar, usually with a sectional dimension of 5 to 20 mm height and 30 to 60 mm width, or a circular equivalent, is extruded from a robotically moving nozzle [34]. However, larger cross-sections of 50 mm by 150 mm or more are also feasible [35]. An object is built by filaments being deposited layer by layer. Although global adoption of the technology was initially slow after its invention by Khoshnevis [36] in the second half of the 1990s, it has seen rapid progress since around 2014, with a range of approaches being developed worldwide.

The manner of forming an object introduces potential anisotropy in a printed structure, typically considered in 3 main orientations: u, v, and w, with u parallel to the print direction, v, perpendicular to the print direction in the print plane, and w, perpendicular to the print plane (also often referred to as directions I, II, and III), see Fig. 3. In unreinforced mortars, the anisotropy mainly stems from the interfaces in the v- and w-directions which are non-existent in the u-direction [37–39]. However, when fibers are added, an additional source of anisotropy is introduced by the non-random fiber distribution. This should be considered when studying 3DP-ECCs.

In 3DCP, the fluid mortar is commonly transported to the nozzle through a flexible hose connected to a progressive cavity pump. In some research set-ups, peristaltic pumps, ram-extruders, auger pumps, caulk guns, or gravity induced flow, are used. Both gantry type robots and industrial arm robots are used, but this seems to have limited influences on the properties of the printed material (although there are operational effects). Industrial scale facilities generally have a reach of

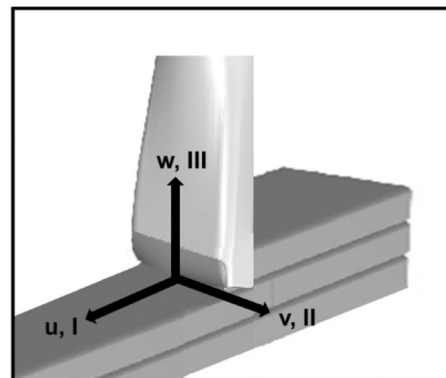


Fig. 3. Defining the u, v, w-directions (or I, II, III-directions).

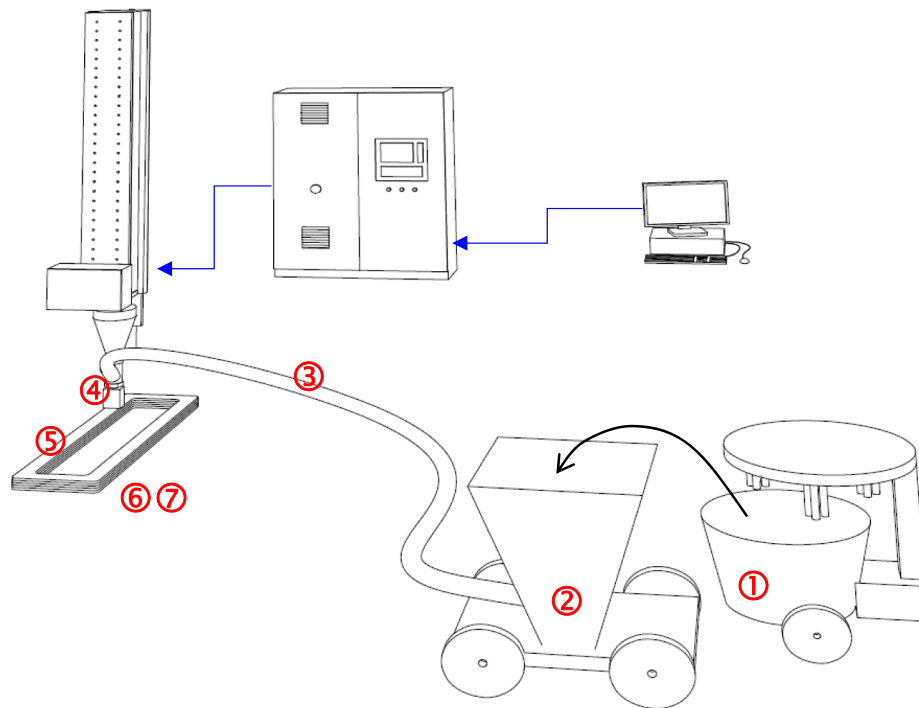


Fig. 4. Schematic representation of the concrete 3D printing process. The numbers correspond to the stages of 3DCP as discussed in the text: 1. Mixing, 2. pumping, 3. transporting, 4. extruding, 5. building, 6. curing, 7. hardened.

several meters in each direction. Some facilities reach up to 10 m in one direction of the print plane. Research facilities of around 1 meter reach are also commonly used, although the maximum build height is generally smaller in those cases. Both batch mixing and continuous mixing processes are being employed. The material can be a one-stage mix (i.e. all constituents are mixed in a single process) or a two-stage mix in which a thixotropic agent or accelerator is added just before extruding the filament. Nozzle ends are sometimes rectangular, and in other cases round with the opening either pointing down or backwards respective to the printing direction. Customized solutions between these types also exist.

The technology requires printable mortars with specific physical properties, the background of which is extensively discussed in [40]. Steps are made to link qualitative concepts that indicate the different aspects of printability of a mortar, such as pumpability, extrudability, and buildability, to quantifiable physical properties. In the context of this paper, the 3DCP process is presented as a sequence of stages undergone by the print mortar, which are related, for a large part but not entirely, to the physical processes. These stages are (see Fig. 4):

1. Mixing – Mixing the dry constituents, additives, and water to prepare the fresh mixture (Section 4.1)
2. Pumping – Feeding of the fresh mixture through a pump so that pressure is built up, pushing the material through the extrusion system (Section 4.2)
3. Transporting – The process of movement of the fresh material from the pump to the print nozzle (Section 4.3)
4. Extruding – Process of depositing filament of fresh material by extrusion through a robotically driven print nozzle (Section 4.4)
5. Building – Process of additively joining layers of filament to form a print object, without the use of formwork (Section 4.5)
6. Curing – Solidification of the printed object through chemical reactions (Section 4.6)
7. Hardened – Condition of the printed object after curing (Section 4.7).

For each of these stages, the use of ECC compared to unreinforced mortars requires specific attention. In Section 4, we will discuss the relations between the 3DCP process and ECC in-depth, by following these stages step-by-step.

3. Current research in printable ECC

Fiber reinforcement has been identified as a potentially suitable means to overcome the brittle failure behavior of printable mortars. A range of studies has been performed on different scales to assess the tensile strength, compressive strength, interlayer bond and ductility of 3D printed concrete with various types of fibers, including steel, glass, basalt, and polypropylene [39,41,43,44]. In most cases, fiber orientation parallel to the filament print direction is observed, often coinciding with increased tensile strength in this direction [39,41,43,44]. Except for mortars specifically designed as ECCs which will be discussed below, no strain hardening behavior has been reported in these fiber-reinforced printed concretes, which tend to show the more common tension-softening response under uniaxial tensile loading.

Recognizing the potential of ECC to address the structural shortcomings of printable cementitious mortars, several groups had set out to develop printable versions of ECC (Table 1). The first results were published in the years 2018–2019.

Soltan & Li [12] developed a mixture based on ordinary Portland Cement (OPC), fly ash and calcium aluminate cement, with various forms of silica as aggregates, viscosity modifiers (nanoclay and high-performance methylcellulose (HPMC)) and superplasticizer admixtures. It contained 2 vol% of 12 mm polyvinyl alcohol (PVA) fiber. To assess printability, the mixture was extruded using a manually operated caulk gun. Printed specimens showed 2–4 MPa direct tensile strength, and 2–4% failure strain. Researchers from the same group later presented a study [21] on functionally graded ECC in which conventional ECC was alternated with photocatalytic ECC. The conventional ECC in this subsequent study had a similar composition, but contained shorter, 8 mm PVA fibers. Nevertheless, similar ultimate strain values (2.4–3.6%) and slightly higher tensile strength of printed specimens (4.7–5.5 MPa)

Table 1
Studies on tensile properties of 3DP-ECC.

Authors	Process	Binder	Fiber type	Fiber length [mm]	Fiber content [%]	Tensile strength [MPa]	Tensile ductility [%]	Remarks
Soltan & Li [12]	Caulk gun	OPC, FA, CAC, silica sand, VMA (NC & HPMC), SP	PVA	12	2	2–4	2–4	Bead diameter 8–13 mm
Bao et al. [21]	Caulk gun	OPC, FA, CAC, silica sand, VMA (NC & HPMC), SP	PVA	8	2	4.7–5.5	2.4–3.6	Photo-catalytic surface
Yu & Leung [18]	Caulk gun	OPC, FA, silica sand, VMA, SP	PVA	12	2	2.5–3.5	5–6	Extruded into molds
Chaves Figueiredo et al. [19,45]	Gantry with down-flow nozzle	- OPC, slag, limestone aggregates, VMA, SP; - OPC, FA, limestone, sand aggregates, VMA, SP	PVA	8	2	1.5–2.5	0.05–0.15	Rect. extrusion mouth (40 × 310 mm)
Ogura et al. [20]	Gantry with rect. nozzle	OPC, silica fume, FA, sand aggregates, SP	HDPE	6	1–1.5	4–5	1–3	Rect. extrusion mouth (30 × 318 mm) Specimens cut from 3DP 80-cm high wall
Zhu et al. [17]	Gantry with down-flow round nozzle	OPC, FA, SAC, silica sand, VMA (NC & HPMC), SP	HDPE	12	1–2	~5 Flexural strength 13–19 MPa	3.6–11.4	Nozzle diameter 20 mm

OPC: ordinary Portland Cement; FA: fly ash; NC: nanoclay; CAC: calcium aluminate cement; VMA: viscosity modifying agent; HPMC: high performance methylcellulose; SP: superplasticizer; SAC: sulfoaluminate cement.

were reported.

Alternatively, Yu & Leung [18] used 2 vol% 12 mm PVA fiber in a mixture with OPC and fly ash binders in a ratio of 1:4, and sand aggregate. Superplasticizer and an unidentified viscosity modifier were applied as well. Similar to [12], the mixture was extruded by a manually operated caulk gun, which had an opening of 10 mm. The mixture was extruded into molds, and therefore may have microstructures, in particular the fiber orientation, different from those of mold-free 3D printed material. In-mold extruded samples of two layers were subjected (among others) to tensile tests parallel and perpendicular to the extrusion direction. In the parallel direction 5–6% failure strains were found at 2.5–3.5 MPa tensile strength, while for the perpendicular direction failure strains of around 2% were found at 1.3–1.9 MPa tensile strength. Notably, the achieved failure strain in perpendicular direction is remarkable as it is commonly assumed fibers cannot bridge the filament interfaces in printed concrete. We suggest that this may have been caused by the presence of the mold and the resulting wall effect on fiber orientation. The orientation of the interfaces (vertical in this case, instead of horizontal) in combination with the viscosity of the mixture, may also have played a role.

Another study that used 2 vol% 8 mm PVA fibers was presented by Chaves Figueiredo et al. [19,45]. Two mixture concepts were developed into printable variants, one based on OPC and blast furnace slag binders and limestone aggregate, and another based on OPC and fly ash binders, and limestone and sand aggregates. Both used viscosity modifier and superplasticizer. Rectangular wall objects were printed in both materials on a large-scale gantry facility, using a down-flow nozzle with a rectangular extrusion mouth (40 mm by 10 mm) connected by a 10 m hose to a progressive cavity pump. An extensive test program on mechanical properties was performed, including four-point bending tests on specimens of different height-to-span ratios, CMOD (Crack Mouth Opening Displacement) tests, and tensile tests in 3 different directions. Generally, the ductility was rather low. Nevertheless, some important results were found. Both mixtures had failure strains of around 0.3–0.5% (hardening) in direction *u* (print filament longitudinal direction), but failure strains of approximately 1.0% in direction *v* (in the print plane, perpendicular to print direction). The authors attribute this to the fiber orientation, see further discussion in Section 4. In direction *w* (perpendicular to print plane, commonly vertical), the failure strain was much lower, as expected, reaching only 0.05–0.15%. However, fracture did not occur through the layer interface, but through the bulk material. The tensile strength (direction *u*) of the OPC-blast furnace slag mixture was 1.5–2.5 MPa, whereas the OPC-fly ash mixture only reached 1.0–1.5 MPa.

Other groups have developed ECCs based on high density polyethylene (HDPE) fibers. Ogura et al. [20] introduced a mix design with cement, silica fume, and fly ash binders (75:15:10 ratio), sand aggregate, and superplasticizer. Short 6 mm HDPE fibers in different volume percentages were used. Printing was performed using a gantry system. The back-flow printing rectangular nozzle was connected to a progressive cavity pump by a short pipe. Linear wall objects were produced, 30 mm wide and 120 mm high. From these walls, specimens for tensile testing in the filament direction were obtained. Strain capacities of 1–3% were obtained at 4–5 MPa tensile strength for 1.0 and 1.5 vol% fibers, respectively. A comparison with mold-cast specimens produced of the same ECC showed that the strain-hardening characteristics of printed specimens were superior to those of mold-cast specimens. In a subsequent study by the authors, 80-cm high straight walls were printed in one session with time intervals of 3 min between individual layers. The specimens for tensile tests were saw-cut in the direction of printing and in the perpendicular direction. The latter specimens exhibited several interlayer joints oriented perpendicular to the uniaxial tensile loading direction. The failure occurred in one of the joints; no strain-hardening was observed. In contrast, the specimens tested in the direction of printing yielded results in agreement to those published in [20] for the same mixture composition and printing

regime.

Zhu et al. [17] also used 12 mm HDPE fibers in a matrix of which the mixture shows similarities with [12], as it is made out of OPC, fly ash, and industrial solid waste-based sulfo-aluminate cement (40:57:3 ratio). Varying fiber quantities were applied, ranging from 1 to 2 vol%. Again, fine silica sand, nanoclay, HPMC, and superplasticizer admixtures were used. A large-scale gantry-based printer with the print area of 3 m × 2 m and the height of 3 m was used to print a slab of 400 mm wide, 400 mm high and 4 layers deep (52 mm), which was used to extract the prismatic and dog-bone samples for material property tests. For the printing process, a round 20 mm diameter nozzle with a downward mouth opening was designed. Remarkable tensile failure strains in the filament direction were reported: 3.57% for 1 vol% fibers, 9.57% for 1.5 vol% fibers and 11.43% for 2 vol% fibers, the tensile strength of approximately 5 MPa, the compressive strength of 47.5–51.1 MPa and the flexural strength of 13.2 MPa–19.4 MPa. It was found that the uniaxial tensile performance of the 3D printed ECCs was superior to that of the conventionally mold-cast ECCs due to aligned fiber orientation and the distribution of pores with more uniform size resulting from the 3DP process.

It should be noted that the brief overview of available studies on 3DP-ECC represents a rough comparison, to obtain insights into the current state of the art. Different groups have used varied materials, both in terms of constituents for the matrix and fiber. Also, a range of test methods have been used, and not all tensile tests, for instance, have been performed identically. Additionally, the characteristics of the print facility vary widely between one study and the other. We suspect this could have a considerable impact on the observed behavior. Nevertheless, these studies seem to confirm that printable ECCs can be developed, i.e. meet the specific requirements related to the printing process, such as pumpability, extrudability, and buildability – from a range of matrix constituents. Although their binder content is generally higher than that of printable mortars without fibers (e.g. [46–48]), they do not diverge widely from other ECC formulations. They can feature strain hardening behavior and significant strain capacity when tested in direction *u* (along filament direction). For directions *v* and *w*, hardly any data are available. There is cause for concern that significant ductility in direction *w* is not obvious to achieve, whereas direction *v* calls for less concern, since tensile/flexural loading in this direction is unlikely to occur in most applications. The interaction between the 3DCP process and ECC performance is further discussed in the following section.

4. Process and performance interaction

4.1. Mixing

Continuous mixing and batch mixing have both been applied in 3DCP. Considering the time dependency of several material properties and the amount of mixture prepared, the latter is more suitable for small scale applications. In large-scale or industrial application, batch mixing introduces undesirable discontinuities in material properties and print quality. When mixtures are developed with increased thixotropy and reduced setting time to increase buildability, it may become difficult to overcome time-dependency effects by continuously shearing a batch after preparation, before pumping through the system. Larger prints would also require multiple batches to be prepared, which raises logistical problems. Continuous mixture preparation therefore seems to be more appropriate from a large-scale print process perspective.

ECC generally require extensive mixing time (minimum of 5 min or more) for proper dispersion of particles and fibers, and for admixtures such as viscosity modifiers to take effect. Pre-mixed dry batches can only partially reduce mixing time. Continuous mixer-pump systems that are used in 3DCP today, such as the M-Tec 2000, enables mixing time to be no more than a few minutes, much too short for ECC. Current studies therefore have all used batch mixing. For large-scale applications in

3DCP, specific equipment and mixing protocols would need to be developed.

Several studies [49–53] have highlighted the influence of the mixing protocol on the mechanical performance of ECC. These studies usually investigate the order that the raw materials are incorporated in the mixing drum, the type of materials which are being used, and the duration of each of the mixing phases.

The importance of the rheological properties of the material on the final mechanical performance was extensively investigated by Şahmaran et al. [49]. From this study, the authors concluded that the total amount of superplasticizer is the key factor to control the fresh properties of ECC. From the same investigation they also observed that the sand-to-binder ratio and the maximum aggregate size had minimal influence on the fresh state but worsened the ductility of the composite. Moreover, Felekoglu et al. [50] investigated, among other variables, the influence of the rheological properties and the machinery used for mixing the composites. They concluded that very workable mixtures are not ideal for ECC as they led to poor fiber distribution. Further, they demonstrated the importance of long mixing time, higher speed and a higher machine torque. Li & Li [51] found that an optimal viscosity controlled by the addition of VMA is important for good fiber dispersion. In [52], the test results showed that the composites mechanical performance could be improved by partially replacing fly ash with blast furnace slag. It was noted that fly ash was essential in ECC as it contributed to improving the rheology and lower the fiber/matrix chemical bond. In [53], an ECC composition rich in limestone powder and blast furnace slag was used to investigate the influence of the mixing procedure in the fiber distribution and mechanical performance of the composite. The authors concluded that a mixing protocol in four stages resulted in the best fiber distribution and consequently improving ECC ductility.

The available literature shows that ECC's mechanical performance depends highly on the mix rheology and mixing protocol employed, which influence the fiber dispersion uniformity and the composite tensile ductility. When material ingredient and mix procedure parameters are combined with 3D print parameters, the number of variables governing the printability of ECCs can increase significantly. Studies assessing the influence of each of the mixing parameters to the overall performance of printable ECC are needed for mastering the technique.

4.2. Pumping

In 3DCP, two approaches have been applied to obtain material behavior allowing object shaping without formwork; either a thixotropic formulation resulting in relatively high stiffness directly after mixing/pumping (no-slump) is used [34,35,46–48] (generally these mixtures are thixotropic resulting in further structuration after deposition), or a less viscous mixture is pumped until it reaches the print head, at which point, a cement hydration accelerator or viscosity modifier is injected into the mix shortly before deposition [54]. The two-stage approach requires less pumping pressure and energy, therefore, bears less risk of clogging the pump. However, this complicates the printer head design with an additional (dynamic) mixing unit to inject and distribute the phase-changing agent through the print mortar. This approach may result in lower shape stability directly after deposition in the first few seconds. Depending on the dosage of the accelerator, the two-stage approach may increase the risk of weak layer-to-layer joints. This is due to rapid increase of deposited layer's stiffness prior to the subsequent layer deposition. The two-stage approach has not yet been applied to printable ECC.

The progressive cavity (PC) pumps that are often used in 3DCP are capable of generating a considerable amount of pressure – up to several dozen bars directly behind the pump. However, to achieve this, the cavity space between the rotor and stator of such pumps is very narrow (order of several millimeters). This is usually not a problem for ECC since the aggregates used are very small ($d < 2$ mm), but it can pose a

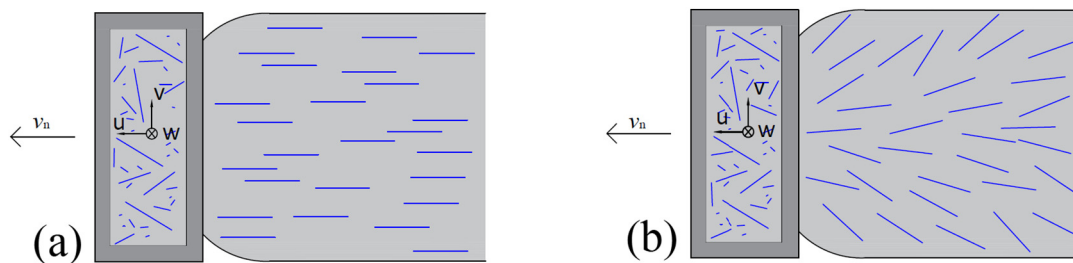


Fig. 5. Generally perceived global orientation of fibers in 3DP-ECC parallel to the print path (a), and global fiber orientation in 3DP-ECC suggested by [45].

problem for the polymer fibers, which often have a length of 8 to 12 mm. Their flexible nature may nevertheless allow them to pass through, but extreme care has to be taken that they are finely dispersed throughout the mix as clogged fibers may block the printer pump. Nevertheless, these pumps have been successfully applied by Ogura et al. [20] and Chaves Figueiredo et al. [19]. In small scale studies, several researchers have used ram-extrusion (i.e. caulk guns) or auger extruders, thus avoiding potential compatibility issues between pump and mixture. However, it is not yet clear whether ram-extruders are applicable for larger scale applications, especially considering their discontinuous nature (extrusion needs to be stopped to refill the cylinder). Peristaltic pumps have also been utilized, as their larger inside diameter and ease of cleaning provide a robust option. One drawback of the peristaltic pump is the significant pulsation of the flow during the pumping process. This can be addressed partially by using a hydraulic accumulator or inline pulsation dampener, or by utilizing a two-stage system of a peristaltic supply pump feeding a PC dispensing pump directly at the point of extrusion [55].

While pumping in relation to 3DP-ECC has not been systematically investigated, such studies have been conducted on ECC mixtures intended for wet-mixture shotcreting. Kim et al. [56] found that the desired pumpability of ECC (defined as pump through without exceeding the maximum spiral pump pressure capacity) can be achieved by controlling the range of solid ingredients loading. This is achieved by mediating the interactions between cement particles with the proper admixtures (SP, HPMC and calcium aluminate particles) and by deliberate addition of mix ingredients in sequence such that the viscosity increase of fresh ECC is controlled during pumping. Secrieru et al. [59] found that the pump pressure of ECCs mainly depends on the tribological yield stress parameter τ_{0i} and tribological viscosity parameter μ_i of the lubrication layer that is formed at the interface between ECC and the wall of a pipe, rather than directly on the rheological parameters such as yield stress and plastic viscosity of the ECC bulk.

4.3. Transporting

The phenomena regarding the pump-induced transport of concrete and cementitious mortars have been discussed, among others, by [40,57,58]. The length over which the mortar can be transported from the pump depends on the flow behavior of the mortar, pumping circuit parameters such as pipe line geometry, as well as friction created between the mortar and hose. Note that if no reservoir is used in the print head, then the nozzle system can play a more significant role in defining the pumping pressure losses. The pipe/wall friction is determined by the internal surface or lining of the hose, the hose diameter, and the internal nozzle geometry. Furthermore, depending on the plastic viscosity and yield stress, printable mortars may be fully sheared during transport, or develop plug-flow, or may develop a lubrication layer between the hose surface and the core of the mortar. Such a layer reduces the pipe/concrete friction and may thus result in longer transport distances for the same initial pressure. Secrieru et al. [59] investigated pumping behavior of ECC with a consistency often reported for this group of materials. The authors observed a tendency of ECC to develop

a relatively thin lubricating layer and distinct plug-flow character.

A general mechanism for the formation of lubrication layer and shear/plug regimes is shear induced particle migration (SIPM). In addition to internal migration of particles, SIPM may also influence the distribution of fibers, which may in turn determine hardened-state properties. This topic remains practically untouched experimentally for 3DCP in general and 3DP-ECCs in particular. However, as the lubrication layer is generally thin in ECC, the effects of SIPM on fiber orientation may actually be limited, and be overridden by shearing effects in the nozzle, prior to extrusion.

4.4. Extruding

After transport of the fluid mixture, the actual filament is created by extrusion at the nozzle. The extrusion process has a vital impact on the deposited material both in fresh and hardened state, especially for fiber enhanced mortars, because it determines the final fiber orientation. It is generally reported that fibers in printed concrete orientate themselves in the longitudinal direction of the filament [39,41,44]. Detailed studies, however, indicate that the reality is more complex: particularly highly flexible fibers, such as the PVA and HDPE fibers used in ECCs, seem to orientate in the principal direction of flow. Initial results presented by Chaves Figueiredo et al. [45] show fibers mainly orientate themselves diagonally in the u,v -plane, as a V-shape behind the nozzle, rather than parallel to the print path (Fig. 5). This flow is non-homogenous at the print head exit. Rather, the friction along the inside walls of the nozzle as well as the lack of confinement along the nozzle edge upon exiting, cause differential flow velocities and directions that can orientate fibers in excess of 45° to the filament direction. In small-scale ceramic printing, rotating nozzles have been suggested to manipulate the filament flow in a way that results in a more isotropic fiber distribution [61]. These observations call for scrutiny in print head design for additive manufacturing with ECC. Nozzle design, an aspect hitherto underappreciated, serves as a potential tool to increase the degree of isotropy in printable ECC.

Ogura et al. [20] quantified extrudability by means of a ram extruder. The results showed that the ease of extrusion increases with decreasing sand/binder ratio in ECC. At a constant sand/binder ratio, ease of extrusion increases with lower ECC viscosity.

The development of extrudable ECC is not something new for the academic world. In the 2000s some research groups have dedicated attention to the extrusion of prefabricated elements and sometimes aiming at strain-hardening performance when loaded in tension [62–64]. This was the case of the study [62,64] where extruded pipes were manufactured based on the development of a fiber reinforced mortar. The groups successfully showed that the pipes could deliver a ductile performance. Moreover, in the study of [63] the authors have also explored the development of extrudable ECCs. In that case, the authors explored the influence of the use of different amounts of chemical admixtures and different types of fibers as well as their aspect ratios. Not only was the mechanical performance of the composites evaluated, but also their rheological properties were assessed with the help of a ram extruder.



Fig. 6. Twisted column, 3DP ECC, University of Michigan.

Quantitative investigation using ram extrusion has been conducted on the extrudability of plastics, ceramics, and cementitious materials [65]. The assessment of rheological properties increases the chance of success in developing new materials for 3DCP [19]. This technique can visually and quantitatively demonstrate the influence of the proportions of raw materials used in the development of the material to be printed. Nevertheless, it remains necessary to match the solid suspension content of the material being extruded with the print speed. This fine tuning ensures that the extruded filament will preserve its shape after being extruded.

Fiber orientation is heavily influenced by the ratio of fiber length to extrusion opening size. Typical filaments in 3DCP are between 5 and 20 mm high, while PVA and HDPE fibers are generally between 8 and 12 mm long. Because of the wall effect, it is therefore practically impossible to obtain a vertical fiber orientation (*w*-direction) with such dimensions for extrusion openings.

As the wall effect causes fibers not to cross the printed filament interfaces, an obvious concern in 3DP-ECCs is retaining crack bridging/ductility across the interfaces. By adjusting the extrusion mouth opening, this may be addressed. This concern is further discussed in Section 4.7.3.

Another important aspect of the extrusion process is synchronization with dynamics of the gantry or robot system. Ideally, the velocity of the nozzle (print head movement) should be constant in relation to the pumping system. In reality, however, this is difficult to achieve, particularly with complex print path geometry. A lack of synchronization will cause variations in the cross-section or width of the extruded bead. Synchronizing a PC feed pump is relatively straight forward, but depending on the length of transport and material properties, this will still result in a significant delay in flow response. This becomes even more critical in layer-based approaches that require precise start and stop behavior for the printer. One approach that has been demonstrated [54] [55] is the use of a supply pump in pressure control mode which feeds a servo-driven progressive cavity pump directly at the extrusion point. The supply pump simply tries to maintain constant inlet pressure to the PC pump. The latter is precisely synchronized to the motion control system of the printhead (gantry or robot), allowing for flow response time on the order of tens of milliseconds.

4.5. Building

3D printing implies the formation of objects without a mold or formwork (although temporary support elements are sometimes used). This renders the print object prone to deformation or collapse during the printing process. In 3DCP, two competing failure mechanisms have been identified: material failure and structural stability failure [66–68]. These are governed by the fresh state material strength and apparent Young's modulus, as well as the slenderness of the built object.

Although the appropriate strength criterion for fresh print mortars is still a topic of academic debate, it is generally assumed both the strength and rigidity are isotropic properties. In fresh ECCs, however, they could be anisotropic due to the fiber orientation – although the extent of which may be time dependent, based on fiber orientation growing in an increasingly rigid state where the fibers will gradually become more effective. Studies in this area are currently lacking. Hitherto developed experimental methods for fresh properties such as strength, rigidity, and flowability (including slump-flow, ram-extrusion, rotational rheometry, shear, and compression tests) are all based on assumed isotropy of the mixture.

The ‘buildability’ of the developed print mortars was demonstrated differently in various research groups, due to the fact that fast setting aluminate cements were used in some mixtures, but not in others. Yu & Leung [18] “printed” in molds, thereby bypassing this issue. Bao et al. [21] and Ogura et al. [20] printed small linear wall elements (the latter, up to 120 mm high). Figueiredo et al. [45] printed linear walls up to 4 layers (of 1 cm), and a cylinder up to failure, initiated at 14 layers. Zhu et al. [17] printed to 17 layers with two mixtures, one of which seemed to show significant deformations at that time.

Most recently, the scale of printing ECC was taken to a new level by researchers at the University of Michigan, which produced a twisted column of about 150 layers that reached a height of approximately 1.5 m (Fig. 6). This column was printed using a typical ECC mix design with 2 vol% PVA fibers, 8 mm in length. The mix was tuned to almost zero slump under a block of 600 g and produced in batches of 15 L to reduce delay in placement. The column was designed to test both buildability with overhanging geometry as well as the start/stop behavior of the overall system, as the middle section of the column bifurcates and rejoins twice as it twists. A peristaltic pump was used to transport the ECC material in a hopper through a flexible hose to an end-of-arm mounted servo-driven progressive cavity pump that extruded the material through a nozzle. The extrusion system also utilized a shaping nozzle to improve the surface quality. The 150 layers (10 mm in height and 25 mm in width) were printed in approximately 2 h, yielding an approximate vertical building rate of 1.25 cm/min. This is comparable to the scale of 3D printed parts that have been fabricated with unreinforced mortars.

4.6. Curing

One of the challenges in 3DCP is to ensure proper curing for printed elements. Extruded filaments are often exposed to environmental effects for prolonged periods without any type of mechanical protection or surface treatments such as plastic covers, wet blankets, or the use of curing compounds. Additionally, the lack of formwork also exposes larger surface area of the material, facilitating the evaporation of the mixing water. Those factors might contribute to larger porosity and eventual cracks that can decrease the mechanical performance or the service life of a given structure.

Proper curing is essential to preserve the best performance of ECCs. In [50], the influence of curing is discussed and the authors emphasized the importance of an adequate curing process to achieve high ductility, strain hardening behavior and generation of small cracks during tensile tests.

Printable mortars generally contain high amounts of cement and relatively low water-to-binder ratios. The use of large volumes of fine

materials is a common characteristic of pumped cementitious materials and ECCs. The use of fine aggregates as well as large contents of binder is crucial to deliver the high ductility as shown in [70,71]. Consequently, they exhibit pronounced autogenous shrinkage. Furthermore, without formwork, 3DCP is exposed to desiccation resulting in plastic and drying shrinkage, unless the print objects are suitably protected (in the case of plastic shrinkage this means protective measures during printing process already). All three types of shrinkage can induce crack formation. Although this topic has not yet been studied in the context of 3DP-ECC, the use of ECC is beneficial as the self-reinforcement reduces autogenous shrinkage crack widths. The finely distributed polymeric fibers in ECC proved to be effective in mitigating plastic shrinkage cracking [69].

Plastic shrinkage is the phenomenon related to the decrease of the volume of cementitious materials due to water loss. The water loss might come from bleeding, evaporation, or cement hydration for example [73]. The high content of small particles in the mixtures lead to small pore size and higher capillary pressures that increases the chances of deformations due to water loss [74,75,77]. In order to mitigate this problem, commonly found in this type of composite, some studies reported smaller drying shrinkage in ECCs which incorporated pre-saturated light weight aggregate [76], partial replacement of cement by supplementary cementitious material [72], or substituting with coarser sand [78].

Assessing the plastic shrinkage of printed elements is crucial as the loss of water of elements built with this type of construction technique is potentially larger than with conventional techniques. Shrinkage problems can be exacerbated by the large amount of fines combined with elevated temperature of the material after extrusion. This is mainly due to the pumping of highly viscous material, causing friction during the material delivery process. Measuring the shrinkage of printed elements will need the use of techniques not usually applied for this purpose. As described in [79], shrinkage measurements are often done using sensors on the surface of the specimen. Lately, new imaging techniques are being used to measure dimensional changes on the specimens [79] or more elaborated investigations reported in [80] where the samples were scanned after printing to create printability indices for comparison.

Despite the above concerns, fiber reinforcement in ECC contributes positively to the mechanical performance of the material in the early age of curing. The fibers can bridge shrinkage-induced cracks, limiting their growth, and influence the overall performance of the printed element.

4.7. Hardened state

4.7.1. Cast versus printed

Comparisons between cast ECC and extruded ECC [12] showed that in-plane (of printed filament) properties (u-direction) tend to be improved, most likely as a result of fiber alignment in the print direction. Fig. 7 shows the enhanced tensile strength and strain capacity of printed ECC over that of cast ECC. This directional benefit of 3DP process on ECC properties was also observed by Yu and Leung [18] and Ogura et al. [20]. Besides the fiber orientation, it may be the case that the extrusion process leads to higher fiber/matrix interface bonds and/or denser ECC due to compaction at the printhead. However, there are currently no definitive experimental data to support this.

It may be noted in Fig. 7 that the first crack strengths of 3DP-ECC specimens are higher than those of cast specimens. Zhu et al. [17], who also found improved strength for u-direction loaded specimens compared to cast specimens, performed SEM (Scanning Electron Microscopy) analysis (20 and 10 μm scale) on their specimens and observed that the total air void content and average air void size was similar in print and cast specimens. However, the range in void sizes was wider for cast specimens, i.e. there were larger as well as smaller voids. They thus concluded that the increase of strength in printed specimens was

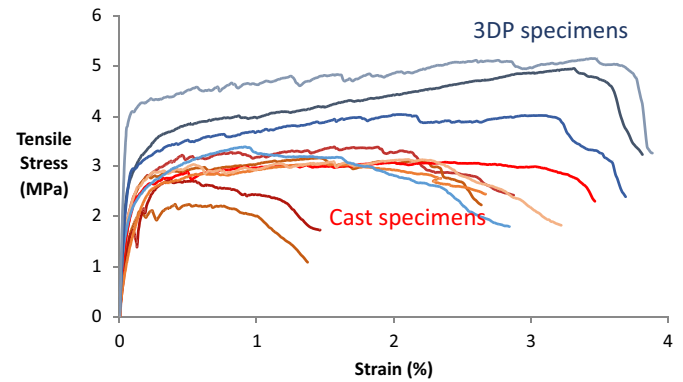


Fig. 7. Tensile properties in the print direction are enhanced by 3DP process when compared with regular cast specimen of the same material composition (after [12]). Data were determined from uniaxial tensile tests on coupon specimens of 305 mm \times 76 mm \times 12.7 mm, with a gage length of 101 mm, following the JSCE testing protocol [28].

due to a reduction of strength-reducing larger voids. One of the possible reasons why this difference in air void size distribution was found might be related to the extrusion process.

Similarly, using a normal optical camera, Ogura et al. [20] qualitatively observed in the fracture surface of tested specimens that there are more large voids in cast specimens than in printed specimens. In that study, reduced strain capacity was observed in cast specimens compared to the printed ones, while the strengths were similar.

Using Eq. (3), it is possible to assess the influence of fiber orientation induced by 3DP on composite $\sigma(\delta)$ relationship, tensile strength capacity σ_0 and complementary energy J_b' . Fig. 8 shows the theoretically computed $\sigma(\delta)$ relationship, normalized by the value σ_0 of the case with fibers orientation (0–90°). Since σ_0 is also the composite ultimate tensile strength, this figure provides a theoretical explanation of the higher ultimate tensile strength in the 3DP specimens when fibers are more aligned in comparison to the case of casted specimens.

Fig. 9 shows the increase in complementary energy J_b' (area to left of each curve in Fig. 8, up to peak load) caused by increasing fiber alignment. This behavior is associated with the larger amount of fiber bridging across the matrix crack. The enhanced J_b' provides the theoretical explanation of the larger tensile strain capacity of the 3DP specimens.

However, contradictory observations were made in the large-scale printing experiment by Figueiredo et al. [45]. They found reduced strength and ductility for printed specimens. The authors partially

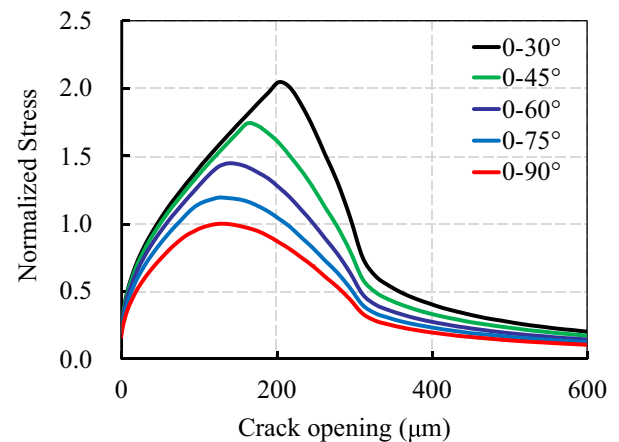


Fig. 8. Computed $\sigma(\delta)$ relationship shows higher tensile strength capacity, doubling when fiber orientation is restricted to (0–30°) when compared to the case of (0–90°).

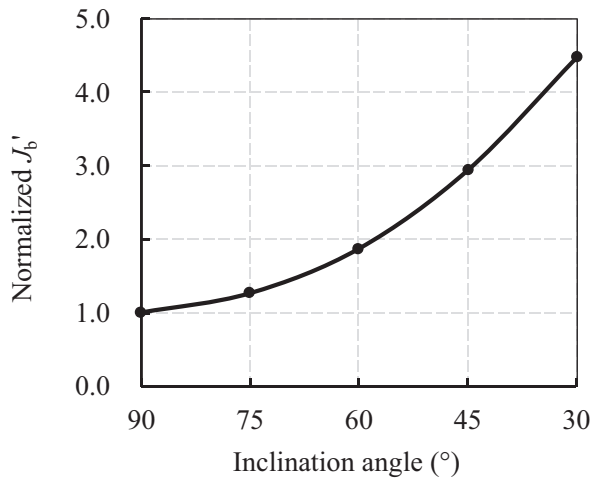


Fig. 9. Complementary energy J_b' for various degree of fiber alignment, normalized by that of the case of (0–90°).

attributed the mechanical performance to higher air void content observed in micro tomography scans with a 7.5 $\mu\text{m}/\text{pixel}$ resolution. Some of the reasons for the lower performance could be related to the large-scale mixing device used to prepare a total volume of 50 L (in two batches of 25 L) together with the extrusion process itself. Besides the fact that the air voids were rounded, the authors pointed out that the long mixing periods could lead to the entrapment of air voids and their spherical shape were facilitated by the chemical admixtures used.

Further research is needed to obtain a better understanding of the effects of the print process on the microstructural properties of ECC.

4.7.2. Anisotropic properties in printed objects

Unreinforced printed concrete is considered isotropic in the bulk material. The layered structure, however, may introduce anisotropy in terms of strength and durability. Recent studies [8] suggest that strength deviations of horizontal interfaces (perpendicular to the height) from the strength of bulk material within the filament may be negligible when the layers are printed within a certain time interval and under the appropriate environmental conditions. Vertical interfaces have hardly been studied.

For ECC, the situation is more complicated. In the (bulk) printed filament itself, the fiber orientation is not random, due to effects discussed in the previous subsections. As a result, both strength and especially ductility should be expected to vary by direction. However, experimental data to support this is scarce. In tension, Yu & Leung [18] found the strength approximately doubled between direction w and u . Meanwhile, the failure strain more than quadrupled. Due to the applied manual print procedure in a mold, these results may have limited quantitative meaning. Figueiredo et al. [40] found the compressive strength to be slightly higher for direction v compared to u (roughly 10%). In uniaxial tension, directions u and v had similar ultimate strengths, although both the initial crack strength and the ultimate strain were higher for direction v . In direction w (across the horizontal interface), the average strength was not impacted when the interlayer interval time was sufficiently short (3 min), and fracture actually occurred through the bulk material. This was explained by the lower air void content shown in the interface area through microtomography scans. As expected, the failure strain in w -direction did fall significantly to the range of 0.05 to 0.15%. Since fracture occurred through the bulk material, this is not directly obvious as it cannot be explained by a lack of fibers crossing the interface. It may be related to the prevalent horizontal orientation of the fibers. Rather, it is assumed the filament flow distributes fibers flatly in the u,v -plane.

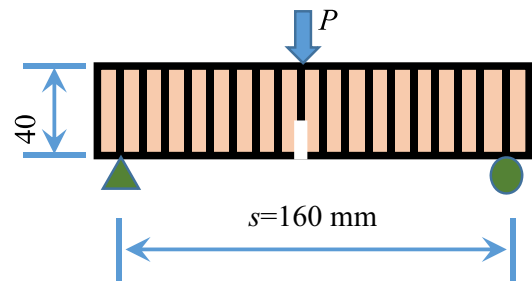


Fig. 10. Single notch test on 3DP-specimen. Initial notch length = 16 mm, specimen thickness is 30 mm.

4.7.3. Horizontal interface

There are few studies on the mechanical behavior of the horizontal interface between adjacent filament layers of 3DP-ECCs. Although intuitively, it may be expected that the lack of fiber crossing the interface will not allow any crack-bridging.

An initial attempt to characterize the interface through single notch fracture tests (Fig. 10) shows the expected brittle failure. However, it appears that a small amount of fibers do penetrate the interface, leading to residual strength after a sudden load drop as shown in Fig. 11(a).

Grooving of the filament can be achieved by use of a corrugated extrusion end-effector [55]. The grooving is intended to generate interlocking effects between adjacent layers. Fracture test show bifurcation of the interfacial crack, leading to a subsequent rise in loading after an initial drop (Fig. 11(b)). This behavior suggests potential further research in toughening of the layer to layer interface that could suppress tendencies of delamination failure.

4.7.4. Durability

Although only a few studies exist that focus on the durability of 3D printed cementitious mortars, these indicate that the layering of filaments can result in higher porosity [82], capillary water ingress [83], and chloride penetration [84], especially when the time interval between subsequent layers increases. To the best of the authors' knowledge, the durability of 3DP-ECC has not yet been studied. The durability of general ECC, on the other hand, has been reported extensively. These studies confirm the high performance of the composite after exposure to freeze and thaw cycles [82,86], sulfate resistance [87], environments with high alkalinity [88], and chloride permeability [89–92]. The explanation for such durability performance is attributed to the small crack widths developed when the composite is loaded in tension [93,94]. Normally the width of those cracks is around 100 μm which, combined with the high binder content and low water-to-binder ratio of the mixtures, leads to a high autogenous self-healing potential [92,96,97]. This potential was furthermore explored with the incorporation of super absorbent polymers to achieve enhanced autogenous self-healing and self-sealing performance [98]. Nevertheless, it remains to be seen whether this favorable behavior can be maintained particularly in the area of layer interfaces, which are not crossed by fibers and may be affected by the lubricating layer.

Functionalized ECC has previously been explored. This includes different strategies [99–101] such as self-healing, self-sensing [103–105], and self-cleaning [102]. Additive manufacturing processes for construction are envisioned to challenge conventional techniques, leading to smarter building practices for the industry. By using material where it is needed, or by strategically placing specific material for different functional purposes, 3D printing could potentially be more economical to use with less waste, all the while, enhancing various performance criteria. Given the higher cost of high-performance materials such as ECC, this process could permit broader use beyond laboratories. An effective and efficient use of ECC [106] highlights why 3DP will improve not only the quality of the built product, but will also transform the way we build with automation for the building sector.

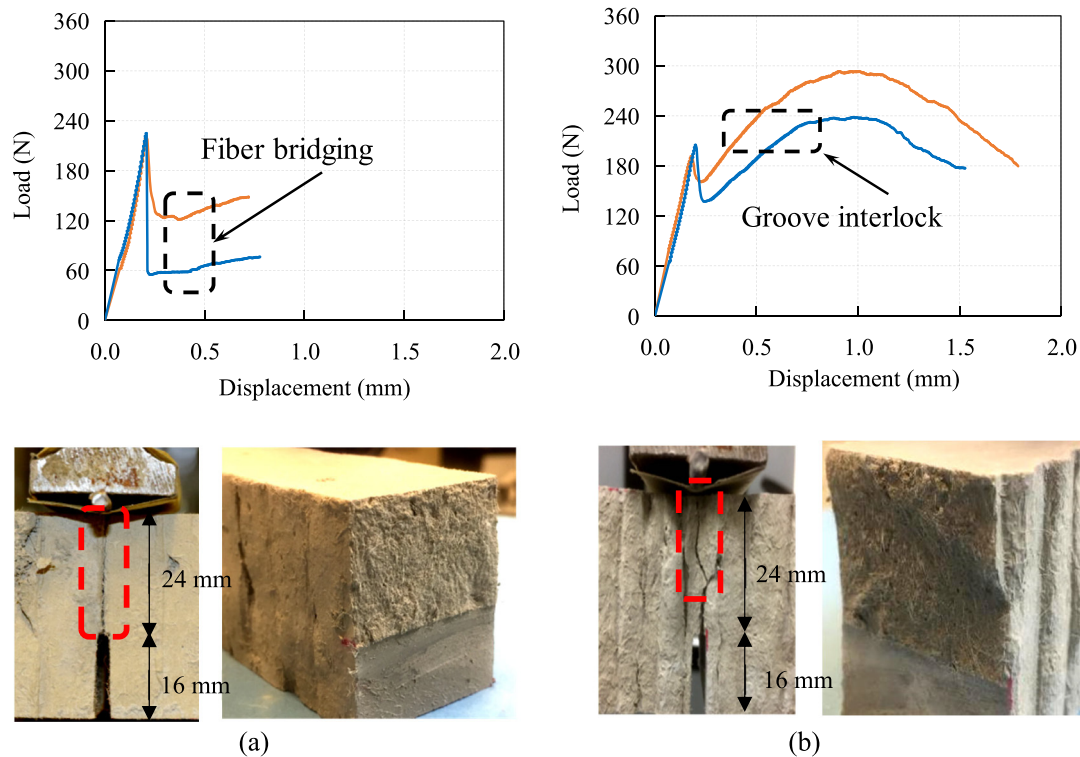


Fig. 11. Fracture behavior of interface for (a) smooth layering and (b) grooved layering.

5. Research priorities

Many research topics in the field of printable ECC remain largely untouched, and deserve attention in the coming years. Nevertheless, we believe some priorities may be identified that relate specifically to the manufacturing of ECC-based objects through the extrusion-based 3D concrete printing technology.

In Section 2, seven stages of the printing process were identified (Fig. 4). In comparison to other uses of ECC, it is particularly stages 4 through 7 in which 3DP-ECC is different – even though there are specific aspects of 3DP-ECC in the preceding stages. However, 3DP-ECC is set apart from 3DCP of unreinforced printed mortars most prominently through its mechanical properties in the hardened state (i.e. stage 7).

The major research areas in 3DCP are outlined in the forthcoming RILEM State-of-the-Art report prepared by the Technical Committee TC 276 Digital Fabrication with Cementitious materials. They include the quantification of printability requirements, such as ‘buildability’, in relation to mixture design process parameters, as well as the effects of printing process parameters have on mechanical and durability performance (also discussed in e.g. [8,106], respectively). The layer interface properties are also receiving specific attention. Such studies are also needed for 3DP-ECC.

Substantial research effort is furthermore put into the use of alternative binders in printable mortars (as well as concrete in general), considering the CO₂ footprint associated with cement [109–111]. Considering that regular concrete uses < 15 wt% solid binders, unreinforced printable mortars contain in the order of 30–45 wt% [82,46–48], while 3DP-ECC requires around 60–70 wt% [12,17–21], it is clear that this topic is particularly relevant for 3DP-ECC. For ECC in general this has already been recognized and low-CO₂ versions of the material have been the subject of several studies [115–117].

The distinctive hardened state properties of 3DP-ECC are largely determined by the synergistic interaction between fiber and matrix via fiber/matrix interface, see Section 2.1. Other things being equal, the distribution uniformity and orientation of fibers play a significant role in the composite tensile properties, particularly the tensile strain

capacity. As indicated in Section 4.4, the extrusion process (stage 4) plays an overarching role in determining fiber orientation. The consideration of anisotropy and heterogeneity introduced by layered extrusion is a major challenge. The interfaces between individual layers are the weakest links with respect to mechanical performance of 3DP-ECC. Approaches on “strengthening” these joints need to be further developed and implemented.

There are several reasons why it is far from trivial to quantitatively determine the fiber distribution and orientation in ECC as a result of the extrusion process. First of all, it should be noted that due to their small diameter and high aspect ratio, polymeric fibers are highly flexible. As a result, they do not remain straight in the matrix material, see Fig. 12. Instead, they are often curved, and sometimes do not lie in a single

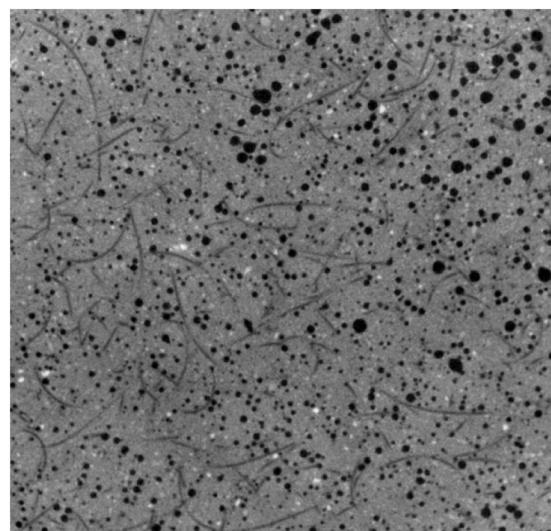


Fig. 12. μ CT scan image of printed ECC, showing the curved PVA fibers (u,v-plane).

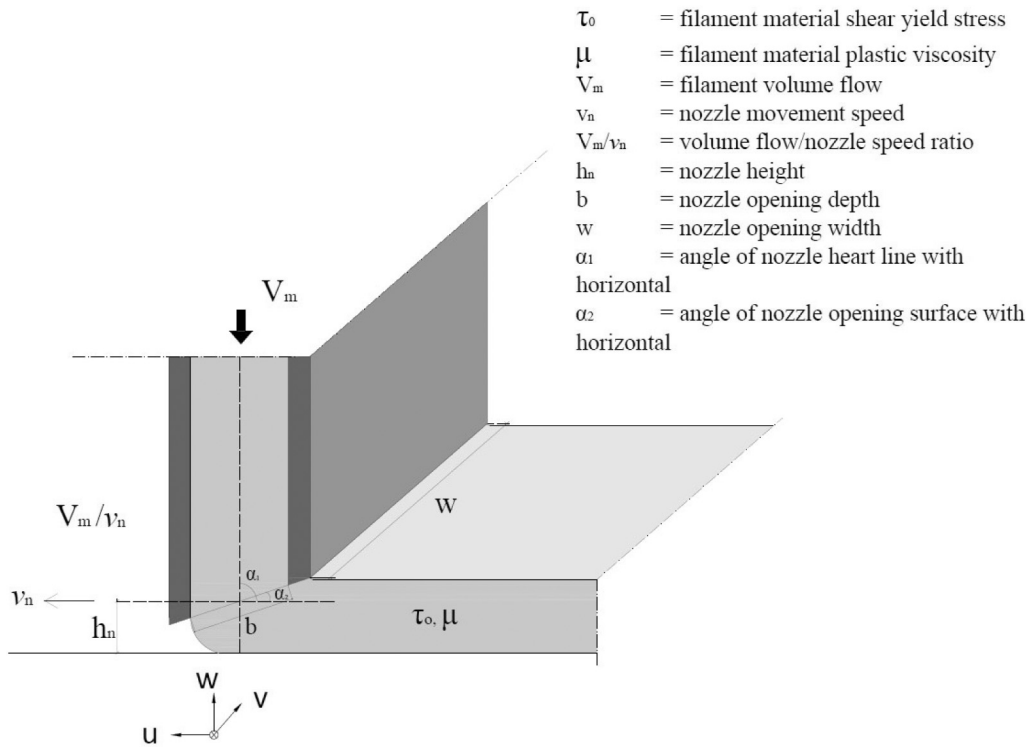


Fig. 13. Illustration of extrusion variables that may influence the final orientation and distribution of fibers.

plane.

When exiting a nozzle, the fiber orientation may be strongly affected by the wall effect, as the short side of the opening is often in the range of 1–3 times the fiber length, whereas the long side is perhaps between 5 and 10 times the fiber length. This means the opening aligns *many* fibers in the principal flow direction, but it is not so tight that it will align *all* fibers in this direction. Subsequently, when exiting the nozzle, this boundary effect disappears and the direction of principal flow steer the fibers to their final location – which will also depend on the time until which the mortar continues to flow (not hindered by formwork). The 3D flow pattern is complex, and depends on the material yield stress and viscosity as well as process parameters such as the ratio of volume rate of material flow to nozzle speed, nozzle opening geometry, the nozzle opening orientation, and the nozzle height above the print surface, see also Fig. 13.

Numerical modeling of the flow of printable mortars exiting a moving nozzle has been studied, e.g. by Comminal et al. [119], and an overview is provided by Roussel et al. [118]. These studies include verifications of volumetric predictions at different volume rate of flow to nozzle speed ratios, but do not include some of the other potential variables, one of the most important variables being the presence of fibers. In an earlier work, Mechtcherine et al. [127] successfully simulated horizontal extrusion of a stiff fiber-reinforced mortar using Distinct Element Method (DEM). The simulation demonstrated a clear reorientation of a majority of the fibers in the nozzle along the direction of the extrusion. The fiber content was relatively low in that study. Ferrara et al. [120] have studied the numerical modeling and verification of the fiber orientation in the casting of a steel fiber reinforced (SFRC) concrete floor. The shear rate vector was shown to be a suitable indicator for the fiber orientation and good correlations were obtained with non-destructive and destructive experimental results. However, the fibers were modeled as rigid ellipsoidal bodies in the matrix and the matrix was highly flowable. Therefore, it should be verified to which extent these conclusions also hold for 3DP-ECC that has a relatively stiff matrix and flexible fibers.

To determine the precise distribution of fibers in the hardened

material is a difficult task. Microscopy observation is limited to a flat plane. 3D X-ray Micro Computed Tomography (μ CT) scanning can be performed. However, the gray scales of the fibers, matrix, and air voids, are hard to distinguish, especially when the fibers are thin. The curving patterns of the fibers is only partial, not a complete image of the whole. Results of fiber orientation presented by Chaves Figueiredo et al. [45] (Fig. 5) are insightful, but insufficient for proper quantitative analysis as they are taken from the 2D u,v-plane and lacks the 3D perspective of fiber orientation. Furthermore, the evaluation of the inclination angle ϕ from the curved fibers is unclear. Only until recently has machine learning algorithms been adopted to model isolated PVA fibers from a three-dimensional μ CT scan. This study, by Lorenzoni et al. [121] however, had constrained fiber orientation since the specimens were cast in narrow molds. Further studies on methods for distributing fibers more randomly in different orientations would be encouraged.

Another issue for consideration is the structural mechanics parameters deduced from or linked to fiber distribution and orientation. The general accepted analytical model reproduced here as Eq. (3), integrates the statistical distribution of fiber orientations relative to the fracture plane, between the found extremes ϕ_0 and ϕ_1 . This approach, however, assumes that the fibers are straight. For fibers that are not straight, the determination of fiber inclination to an arbitrary fracture plane is not straightforward. It will change along the fiber length for parallel planes. The development of an analytical approach to determine an effective inclination angle of curved fibers would be studied. However, it may be difficult to verify. Alternatively, numerical methods could be developed. Bosco et al. [122] rigorously determined the effective macro scale chemo-mechanical properties in concrete by using a multi-scalar approach based on asymptotic homogenization. Such an approach could be adopted to account for non-linear fracture processes and used in combination with μ CT scans to provide accurate fiber orientation locally. If successful, this approach could also be used to check the validity of simpler analytical models for 3DP-ECC properties.

A variety of structural scale tests has been conducted on ECC elements [30,123,124]. Based on a series of increasing size steel reinforced ECC beams, Lepech & Li [125] found that there is little size effect. In

contrast, according to Mündecke & Mechtcherine [30], large ECC slabs (3 m by 1 m by 0.24 m) loaded in direct tension, yielded considerably lower values for tensile strength and strain capacity in comparison to small-scale specimens. Given the lack of structural tests of full scale 3DP-ECC elements, very little is known of structural-scale load response. Flexural tests by Chaves Figueiredo et al. [45] on printed ECC specimens of 1, 2, 3, and 4 layers with identical geometry showed that deflection was reduced as the specimen was built higher. However, other scaling effects may occur in larger elements. There is a need to print and test large-scale 3DP-ECC structural elements to verify the applicability of developed mechanics models and identify possible scaling effects, for instance, as discussed for 3DCP by Bos et al. [126].

Finally, there is a need to investigate the long-term durability of 3DP-ECC material and structure, the latter involving the interface between layers.

6. Conclusions

This review paper surveys the state of the art on 3DP of ECC material, based on limited studies in Asia, Europe, and the United States so far.

Despite the widely different mix designs and 3DP equipment used, the findings collectively confirm that self-reinforcing ECC meets the basic requirements for 3DP. That is, even with the relatively high fiber content of around two volume percent, ECC can be mixed, pumped, transported, extruded, and built. As it stands, it appears feasible to build above 2 m in height without collapse due to buckling or otherwise. However, much remains to be explored in mix optimization and in the details of material-machine interactions.

The printed ECC tends to show anisotropic properties, retaining the tensile strain-hardening behavior characteristic of this class of material in the print filament along the print direction. As expected, the ductility in the filament in the perpendicular directions is substantially lower, particularly in the vertical direction across the (horizontal) interfaces. This anisotropic behavior is not surprising given the extrusion induced fiber alignment in the print direction, although the magnitude of fiber alignment is governed by various print parameters. What may be surprising is that a minimal amount of toughness across the interface between adjacent filaments is nevertheless retained, likely a result of fibers crossing the filaments when printed layers are joined while still in a fresh state. The potential bottleneck of the weaker interface between print filaments remains one that requires attention by researchers, to ensure structural reliability and robustness for full-scale structures.

There remain large areas of needed research in 3DP-ECC structures. These include for example the curing of printed structures, the long-term durability under various environmental exposures, and response to a variety of loading types (static, impact, creep, etc.). The quantitative determination of fiber distribution and orientation as a result of the extrusion process, and the way this is to be incorporated in mechanical models, is identified as a major research priority. When these studies are coupled with large-scale structural tests, true values for 3DP-ECC will emerge.

Declaration of competing interest

The authors declare that there's no financial/personal interest or belief that could affect their objectivity. The authors confirm explicitly that no conflicts of interest exist.

Acknowledgements

The University of Michigan research team would like to acknowledge financial support of 3DP-ECC research by the Department of Civil and Environmental Engineering, the College of Engineering, the Taubman College of Architecture and Urban Planning's Prototyping

Tomorrow Grant Initiative, and the MCubed, University of Michigan 3.0 as well as the Clusters and Theme programs. TU Dresden gratefully acknowledges the financial support of the German Research Foundation (DFG) for funding the Research Training Group GRK 2250 "Mineral-bonded composites for enhanced structural impact safety". The research team of Southeast University would like to acknowledge financial support from National Key Research and Development Program of China (2017YFC0703700). The support by The Concrete Institute and the Technology and Human Resources for Industry Program under grant TP 14062772324 is gratefully acknowledged by the Stellenbosch University team.

References

- [1] V.C. Li, *Engineered Cementitious Composites (ECC)*, Springer, 2019.
- [2] V.C. Li, From micromechanics to structural engineering - the design of cementitious composites for civil engineering applications, *Journal of Structural Engineering and Earthquake Engineering* 471 (1993) 1–24.
- [3] M.D. Lepech, V.C. Li, Application of ECC for bridge deck link slabs, *RILEM J. of Materials and Structures* 42 (9) (2009) 1185–1195.
- [4] M. Hiroshi, S. Kumilko, S. Noboru, H. Takenori, S. Keji, Application of overlay reinforcement method on steel deck utilizing engineered cementitious composites – Mihara Bridge, *Bridge Infrastructure V8* (88–91) (2005) 2005 (in Japanese).
- [5] M. Maruta, T. Kand, S. Nagai, Y. Yamamoto, New high-rise RC structure using precast ECC coupling beam, *Concrete Journal V43* (11) (2005) 18–26 (in Japanese).
- [6] E. Schlangen, M.G. Sierra Beltran, M. Lukovic, G. Ye (Eds.), *SHCC 3 - 3rd International RILEM Conference on Strain Hardening Cementitious Composites*, 03–05 November, 2014 (Dordrecht, The Netherlands).
- [7] V. Mechtcherine, V. Slowik, P. Kabele (Eds.), *Strain-hardening Cement-based Composites SHCC4*, Springer, RILEM Bookseries, 2017.
- [8] T. Wangler, N. Roussel, F.P. Bos, T.A. Salet, R.J. Flatt, Digital concrete: a review, *Cem. Concr. Res.* 123 (2019) 105780.
- [9] D. Asprone, C. Menna, F.P. Bos, T.A. Salet, J. Mata-Falcón, W. Kaufmann, Rethinking reinforcement for digital fabrication with concrete, *Cem. Concr. Res.* 112 (2018) 111–121.
- [10] V. Mechtcherine, J. Grafe, V.N. Nerella, E. Spaniol, M. Hertel, U. Füssel, 3D-printed steel reinforcement for digital concrete construction—manufacture, mechanical properties and bond behaviour, *Constr. Build. Mater.* 179 (2018) 125–137.
- [11] V. Mechtcherine, A. Michel, M. Liebscher, K. Schneider, C. Großmann, Mineral-impregnated carbon fiber composites as novel reinforcement for concrete construction: material and automation perspectives, *Autom. Constr.* 110 (2020) 103002.
- [12] D.G. Soltan, V.C. Li, A self-reinforced cementitious composite for building-scale 3D printing, *Cem. Concr. Compos.* 90 (2018) 1–13.
- [13] K. Yu, L. Li, J. Yu, J. Xiao, J. Ye, Y. Wang, Feasibility of using ultra-high ductility cementitious composites for concrete structures without steel rebar, *Eng. Struct.* 170 (2018) 11–20.
- [14] E.H. Yang, V.C. Li, A.N. Dancygier, D. Yankelevsky, A. Katzb, A. Bentur, Impact resistance of engineered cementitious composites, *International Symposium on Interaction of the Effects of Munitions with Structures (ISIEMS)*, 2007.
- [15] I. Curosu, V. Mechtcherine, D. Forni, E. Cadoni, Performance of various strain-hardening cement-based composites (SHCC) subject to uniaxial impact tensile loading, *Cem. Concr. Res.* 102 (2017) 16–28.
- [16] J. Zhang, M. Maalej, S.T. Quek, Performance of hybrid-fiber ECC blast/shelter panels subjected to drop weight impact, *J. Mater. Civ. Eng.* 19 (10) (2007) 855–863.
- [17] R. Zhu, J. Pan, B. Nematollahi, Z. Zhou, Y. Zhang, J. Sanjayan, Development of 3D printable engineered cementitious composites with ultra-high tensile ductility for digital construction, *Mater. Des.* 181 (2019) 108088.
- [18] J. Yu, C.K. Leung, Impact of 3D printing direction on mechanical performance of strain-hardening cementitious composite (SHCC), *RILEM International Conference on Concrete and Digital Fabrication*, Springer, Cham, 2018, pp. 255–265.
- [19] S.C. Figueiredo, C.R. Rodríguez, Z.Y. Ahmed, D.H. Bos, Y. Xu, T.M. Salet, F.P. Bos, An approach to develop printable strain hardening cementitious composites, *Mater. Des.* 169 (2019) 107651.
- [20] H. Ogura, V. Nerella, V. Mechtcherine, Developing and testing of strain-hardening cement-based composites (SHCC) in the context of 3D-printing, *Materials* 11 (8) (2018) 1375.
- [21] Y. Bao, M. Xu, D. Soltan, T. Xia, A. Shih, H.L. Clack, V.C. Li, Three-dimensional printing multifunctional engineered cementitious composites (ECC) for structural elements, *RILEM International Conference on Concrete and Digital Fabrication*, Springer, Cham, 2018, September, pp. 115–128.
- [22] Q. Zhang, V.C. Li, Development of durable spray-applied fire-resistant Engineered Cementitious Composites (SFR-ECC), *Cem. Concr. Compos.* 60 (2015) 10–16.
- [23] R. Ranade, *Advanced Cementitious Composite Development for Resilient and Sustainable Infrastructure*, University of Michigan, 2014 (Doctoral dissertation).
- [24] K.Q. Yu, J.T. Yu, J.G. Dai, Z.D. Lu, S.P. Shah, Development of ultra-high performance engineered cementitious composites using polyethylene (PE) fibers, *Constr. Build. Mater.* 158 (2018) 217–227.
- [25] D.Y. Lei, L.P. Guo, B. Chen, I. Curosu, V. Mechtcherine, The connection between

- microscopic and macroscopic properties of ultra-high strength and ultra-high ductility cementitious composites (UHS-UHDC), *Compos. Part B* 164 (2019) 144–157.
- [26] I. Curosu, M. Liebscher, V. Mechtcherine, C. Bellmann, S. Michel, Tensile behavior of high-strength strain-hardening cement-based composites (HS-SHCC) made with high-performance polyethylene, aramid and PBO fibers, *Cem. Concr. Res.* 98 (2017) 71–81.
- [27] US Federal Highway Administration, Properties and Behavior of UHPC-Class Materials, FHWA-HRT-06-103, (2018).
- [28] Japan Society of Civil Engineers, Recommendations for design and construction of high performance fiber reinforced cement composites with multiple fine cracks (HPFRCC), Concrete Engineering Series, vol. Concrete L, 2008.
- [29] M. Ranjbarian, V. Mechtcherine, Z. Zhang, I. Curosu, J. Storm, M. Kaliske, Locking Front Model for pull-out behaviour of PVA microfibre embedded in cementitious matrix, *Cem. Concr. Compos.* 103 (2019) 318–330.
- [30] E. Mündecke, V. Mechtcherine, Tensile behaviour of strain-hardening cement-based composites (SHCC) with steel reinforcing bars, *Cem. Concr. Compos.* 105 (2020) 103423.
- [31] G. Fischer, V.C. Li, Influence of matrix ductility on tension-stiffening behavior of steel reinforced engineered cementitious composites (ECC), *Structural Journal* 99 (1) (2002) 104–111.
- [32] G. Parra-Montesinos, J.K. Wight, Seismic response of exterior RC column-to-steel beam connections, *J. Struct. Eng.* 126 (10) (2000) 1113–1121.
- [33] K. Kesner, S.L. Billington, Investigation of infill panels made from engineered cementitious composites for seismic strengthening and retrofit, *J. Struct. Eng.* 131 (11) (2005) 1712–1720.
- [34] F. Bos, R. Wolfs, Z. Ahmed, T. Salet, Additive manufacturing of concrete in construction: potentials and challenges of 3D concrete printing, *Virtual and Physical Prototyping* 11 (3) (2016) 209–225.
- [35] V. Mechtcherine, V.N. Nerella, F. Will, M. Näther, J. Otto, M. Krause, Large-scale digital concrete construction – CONPrint3D concept for on-site, monolithic 3D-printing, *Autom. Constr.* 107 (2019) 102933.
- [36] B. Khoshnevis, R. Dutton, Innovative rapid prototyping process makes large sized, smooth surfaced complex shapes in a wide variety of materials, *Mater. Technol.* 13 (2) (1998) 53–56.
- [37] R.J.M. Wolfs, F.P. Bos, T.A.M. Salet, Hardened properties of 3D printed concrete: the influence of process parameters on interlayer adhesion, *Cem. Concr. Res.* 119 (2019) 132–140.
- [38] V.N. Nerella, S. Hempel, V. Mechtcherine, Effects of layer-interface properties on mechanical performance of concrete elements produced by extrusion-based 3D-printing, *Constr. Build. Mater.* 205 (2019) 586–601.
- [39] B. Panda, S.C. Paul, M.J. Tan, Anisotropic mechanical performance of 3D printed fiber reinforced sustainable construction material, *Mater. Lett.* 209 (2017) 146–149.
- [40] V. Mechtcherine, F. Bos, A. Perrot, W.R.L. da Silva, V.N. Nerella, S. Fataei, R. Wolfs, M. Sonebi, N. Roussel, Extrusion-based additive manufacturing with cement-based materials – processing steps and their underlying physics: a review, *Cement and Concrete Research* (2020), <https://doi.org/10.1016/j.cemconres.2020.106037>.
- [41] M. Hambach, D. Volkmer, Properties of 3D-printed fiber-reinforced Portland cement paste, *Cem. Concr. Compos.* 79 (2017) 62–70, 2017.
- [42] B. Nematollahi, P. Vijay, J. Sanjayan, A. Nazari, M. Xia, V. Naidu Nerella, V. Mechtcherine, Effect of polypropylene fibre addition on properties of geopolymers made by 3D printing for digital construction, *Materials* 11 (12) (2018) 2352.
- [43] F.P. Bos, E. Bosco, T.A.M. Salet, Ductility of 3D printed concrete reinforced with short straight steel fibers, *Virtual and Physical Prototyping* 14 (2) (2019) 160–174.
- [44] S. Chaves Figueiredo, C. Romero Rodriguez, Z.Y. Ahmed, D.H. Bos, X. Yu, T.A.M. Salet, O. Çopuroğlu, E. Schlangen, F.P. Bos, Mechanical behaviour of printed strain hardening cementitious composites, submitted to *Materials*, (2020) Under review.
- [45] S.C. Paul, Y.W.D. Tay, B. Panda, M.J. Tan, Fresh and hardened properties of 3D printable cementitious materials for building and construction, *Archives of Civil and Mechanical Engineering* 18 (1) (2018) 311–319.
- [46] A. Kazemian, X. Yuan, E. Cochran, B. Khoshnevis, Cementitious materials for construction-scale 3D printing: laboratory testing of fresh printing mixture, *Constr. Build. Mater.* 145 (2017) 639–647.
- [47] J. Kruger, S. Zeranka, G. van Zijl, An ab initio approach for thixotropy characterisation of (nanoparticle-infused) 3D printable concrete, *Constr. Build. Mater.* 224 (2019) 372–386.
- [48] M. Şahmaran, Z. Bilici, E. Ozbay, T.K. Erdem, H.E. Yucel, M. Lachemi, Improving the workability and rheological properties of Engineered Cementitious Composites using factorial experimental design, *Compos. Part B* 45 (1) (2013) 356–368.
- [49] B. Felekoglu, K. Tosun-Felekoglu, R. Ranade, Q. Zhang, V.C. Li, Influence of matrix flowability, fiber mixing procedure, and curing conditions on the mechanical performance of HTPP-ECC, *Compos. Part B* 60 (2014) 359–370.
- [50] M. Li, V.C. Li, Rheology, fiber dispersion, and robust properties of Engineered Cementitious Composites, *Material and Structures* 46 (3) (2013) 405–420.
- [51] Y. Zhu, Y. Yang, Y. Yao, Use of slag to improve mechanical properties of engineered cementitious composites (ECCs) with high volumes of fly ash, *Constr. Build. Mater.* 36 (2012) 1076–1081.
- [52] J. Zhou, S. Qian, G. Ye, O. Copuroglu, K. van Breugel, V.C. Li, Improved fiber distribution and mechanical properties of engineered cementitious composites by adjusting the mixing sequence, *Cem. Concr. Compos.* 34 (3) (2012) 342–348.
- [53] C. Gosselin, R. Duballet, P. Roux, N. Gaudillière, J. Dirrenberger, P. Morel, Large-scale 3D printing of ultra-high performance concrete—a new processing route for architects and builders, *Mater. Des.* 100 (2016) 102–109.
- [54] V. McGee, T. Ng, K. Yu, V.C. Li, Extrusion nozzle shaping as an approach for improved 3DP of engineered cementitious composites, *Digital Concrete 2020, Proceedings of the 2nd RILEM International Conference on Concrete and Digital Fabrication*, 2020 Accepted for publication.
- [55] Y. Kim, H. Kong, V.C. Li, Design of engineered cementitious composite suitable for wet-mixture shotcreting, *ACI Mater. J.* 100 (6) (2003) 511–518.
- [56] V.N. Nerella, V. Mechtcherine, Virtual Sliding Pipe Rheometer for estimating pumpability of concrete, *Constr. Build. Mater.* 170 (2018) 366–377.
- [57] E. Secrieru, D. Cotardo, V. Mechtcherine, L. Lohaus, C. Schröfl, C. Begemann, Changes in concrete properties during pumping and formation of lubricating material under pressure, *Cem. Concr. Res.* 108 (2018) 129–139.
- [58] E. Secrieru, V. Mechtcherine, C. Schröfl, D. Borin, Rheological characterisation and prediction of pumpability of strain-hardening cement-based-composites (SHCC) with and without addition of superabsorbent polymers (SAP) at various temperatures, *Constr. Build. Mater.* 112 (2016) 581–594.
- [59] J.R. Raney, B.G. Compton, J. Mueller, T.J. Ober, K. Shea, J.A. Lewis, Rotational 3D printing of damage-tolerant composites with programmable mechanics, *Proc. Natl. Acad. Sci.* 115 (6) (2018) 1198–1203.
- [60] D. De Koker, G.P.A.G. Van Zijl, Extrusion of engineered cement-based composite material, *Proceedings of BEFIB*, 2004, pp. 1301–1310.
- [61] R. Srinivasan, D. DeFord, S.P. Shah, The use of extrusion rheometry in the development of extruded fiber-reinforced cement composites, *Concr. Sci. Eng.* 1 (1) (1999) 26–36.
- [62] H. Stang, V.C. Li, Extrusion of ECC-material, in: H. Reinhardt, A. Naaman (Eds.), *Proc., High Performance Fiber Reinforced Cement Composites 3 (HPFRCC 3)*, Chapman & Hall, 1999, pp. 203–212.
- [63] W. Gleissle, J. Graczyk, Rheology and extrudability of ceramic compounds, *Extrusion in Ceramics*, Springer, Heidelberg, 2009, pp. 161–171.
- [64] R.J.M. Wolfs, F.P. Bos, T.A.M. Salet, Early age mechanical behaviour of 3D printed concrete: numerical modelling and experimental testing, *Cem. Concr. Res.* 106 (2018) 103–116.
- [65] J. Kruger, S. Zeranka, G. van Zijl, 3D concrete printing: a lower bound analytical model for buildability performance quantification, *Autom. Constr.* 106 (2019) 102904.
- [66] J. Kruger, S. Cho, S. Zeranka, C. Viljoen, G. van Zijl, 3D concrete printer parameter optimisation for high rate digital construction avoiding plastic collapse, *Compos. Part B* 107660 (2019).
- [67] I. Serpukhov, V. Mechtcherine, Early-age shrinkage of ordinary concrete and a strain-hardening cement-based composite (SHCC) in the conditions of hot weather casting, *CONCREEP 10*, 2015, pp. 1504–1513.
- [68] L.Z. Li, Z.W. Cai, K.Q. Yu, Y.X. Zhang, Y. Ding, Performance-based design of all-grade strain hardening cementitious composites with compressive strengths from 40 MPa to 120 MPa, *Cem. Concr. Compos.* 97 (2019) 202–217.
- [69] K.Q. Yu, Z.D. Lu, J.G. Dai, S.P. Shah, Direct tensile properties and stress-strain model of UHP-ECC, *J. Mater. Civ. Eng.* 32 (1) (2020) 04019334.
- [70] K.Q. Yu, W.J. Zhu, Y. Ding, Z.D. Lu, J.T. Yu, J.Z. Xiao, Micro-structural and mechanical properties of ultra-high performance engineered cementitious composites (UHP-ECC) incorporation of recycled fine powder (RFP), *Cem. Concr. Res.* 124 (2019) 105813.
- [71] S. Ghourchian, M. Wyrzykowski, M. Plamondon, P. Lura, On the mechanism of plastic shrinkage cracking in fresh cementitious materials, *Cem. Concr. Res.* 115 (2019) 251–263.
- [72] S. Ghourchian, M. Wyrzykowski, L. Baquerizo, P. Lura, Susceptibility of Portland cement and blended cement concretes to plastic shrinkage cracking, *Cem. Concr. Compos.* 85 (2018) 44–55.
- [73] M.B. Weimann, Drying shrinkage and crack width of engineered cementitious composites (ECC), *Brittle Matrix Composites*, 7 Woodhead Publishing, 2003, pp. 37–46.
- [74] M. Şahmaran, M. Lachemi, K.M. Hossain, V.C. Li, Internal curing of engineered cementitious composites for prevention of early age autogenous shrinkage cracking, *Cem. Concr. Res.* 39 (10) (2009) 893–901.
- [75] O.S.B. Al-Amoudi, M. Maslehuddin, T.O. Abiola, Effect of type and dosage of silica fume on plastic shrinkage in concrete exposed to hot weather, *Constr. Build. Mater.* 18 (10) (2004) 737–743.
- [76] Y. Yang, Y. Yao, X. Gao, H. Deng, P. Yu, Shrinkage reducing measures for engineering cementitious composites, *Journal of Wuhan University of Technology-Mater. Sci. Ed.* 23 (6) (2008) 907–911.
- [77] I.M.G. Bertelsen, C. Kragh, G. Cardinaud, L.M. Ottosen, G. Fischer, Quantification of plastic shrinkage cracking in mortars using digital image correlation, *Cem. Concr. Res.* 123 (2019) 105761.
- [78] S. Ketel, G. Falzone, B. Wang, N. Washburn, G. Sant, A printability index for linking slurry rheology to the geometrical attributes of 3D-printed components, *Cem. Concr. Compos.* 101 (2019) 32–43.
- [79] J. Van Der Putten, G. De Schutter, K. Van Tittelboom, The effect of print parameters on the (micro)structure of 3D printed cementitious materials, in: T. Wangler, R.J. Flatt (Eds.), *First RILEM Int. Conf. Concr. Digit. Fabr. – Digit. Concr.* 2018, Springer International Publishing, 2019, pp. 234–244.
- [80] C. Schröfl, V.N. Nerella, V. Mechtcherine, Capillary water intake by 3D-printed concrete visualised and quantified by neutron radiography, in: T. Wangler, R.J. Flatt (Eds.), *First RILEM Int. Conf. Concr. Digit. Fabr. – Digit. Concr.* 2018, Springer International Publishing, 2019, pp. 217–224.
- [81] P.C. Bran Anleu, T. Wangler, R.J. Flatt, Chloride ingress through cold joints in digitally fabricated concrete by micro-XRF mapping, <https://www.researchcollection.ethz.ch/handle/20.500.11850/312939>, (2018), Accessed date: 9 March 2019.

- [86] M. Şahmaran, E. Özbay, H.E. Yücel, M. Lachemi, V.C. Li, Frost resistance and microstructure of engineered cementitious composites: influence of fly ash and micro poly-vinyl-alcohol fiber, *Cem. Concr. Compos.* 34 (2) (2012) 156–165.
- [87] E. Özbay, O. Karahan, M. Lachemi, K.M. Hossain, C.D. Atis, Dual effectiveness of freezing–thawing and sulfate attack on high-volume slag-incorporated ECC, *Compos. Part B* 45 (1) (2013) 1384–1390.
- [88] M. Şahmaran, V.C. Li, Durability of mechanically loaded engineered cementitious composites under highly alkaline environments, *Cem. Concr. Compos.* 30 (2) (2008) 72–81.
- [89] M. Şahmaran, V.C. Li, Durability properties of micro-cracked ECC containing high volumes fly ash, *Cem. Concr. Res.* 39 (11) (2009) 1033–1043.
- [90] K. Kobayashi, D. Le Ahn, K. Rokugo, Effects of crack properties and water-cement ratio on the chloride proofing performance of cracked SHCC suffering from chloride attack, *Cem. Concr. Compos.* 69 (2016) 18–27.
- [91] M. Luković, B. Šavija, G. Ye, E. Schlangen, K. van Breugel, Failure modes in concrete repair systems due to ongoing corrosion, *Adv. Mater. Sci. Eng.* 2017 (2017).
- [92] W.P. Boshoff, F. Altmann, C.J. Adendorff, V. Mechtcherine, A new approach for modelling the ingress of deleterious materials in cracked strain hardening cement-based composites, *Mater. Struct.* 49 (6) (2016) 2285–2295.
- [93] G.P.A.G. Van Zijl, W.H. Wittmann, B.H. Oh, P. Kabele, R.D. Toledo Filho, E.M.R. Fairbairn, V. Slowik, A. Ogawa, H. Hoshiro, V. Mechtcherine, F. Altmann, M.D. Lepech, Durability of strain-hardening cement-based composites (SHCC), *Mater. Struct.* 45 (2012) 1447–1463.
- [94] F. Altmann, J.-U. Sickert, V. Mechtcherine, M. Kaliske, A fuzzy-probabilistic durability concept for strain-hardening cement-based composites (SHCCs) exposed to chlorides: part 1: concept development, *Cem. Concr. Compos.* 34 (2012) 754–762.
- [96] Y. Zhu, Y. Yang, Y. Yao, Autogenous self-healing of engineered cementitious composites under freeze–thaw cycles, *Constr. Build. Mater.* 34 (2012) 522–530.
- [97] J.H. Yu, W. Chen, M.X. Yu, Y.E. Hua, The microstructure of self-healed PVA ECC under wet and dry cycles, *Mater. Res.* 13 (2) (2010) 225–231.
- [98] D. Snoeck, Superabsorbent polymers to seal and heal cracks in cementitious materials, *RILEM Technical Letters* 3 (2018) 32–38.
- [99] Z. Zhang, Q. Zhang, Self-healing ability of engineered cementitious composites (ECC) under different exposure environments, *Constr. Build. Mater.* 156 (2017) 142–151.
- [100] E. Herbert, V. Li, Self-healing of microcracks in engineered cementitious composites (ECC) under a natural environment, *Materials* 6 (7) (2013) 2831–2845.
- [101] M.G. Sierra-Beltran, H.M. Jonkers, E. Schlangen, Characterization of sustainable bio-based mortar for concrete repair, *Constr. Build. Mater.* 67 (2014) 344–352.
- [102] A. Zhao, J. Yang, E.H. Yang, Self-cleaning engineered cementitious composites, *Cem. Concr. Compos.* 64 (2015) 74–83.
- [103] R. Ranade, J. Zhang, J.P. Lynch, V.C. Li, Influence of micro-cracking on the composite resistivity of engineered cementitious composites, *Cem. Concr. Res.* 58 (2014) 1–12.
- [104] Y. Huang, H. Li, S. Qian, Self-sensing properties of Engineered Cementitious Composites, *Constr. Build. Mater.* 174 (2018) 253–262.
- [105] S.C. Figueiredo, O. Çopuroğlu, B. Šavija, E. Schlangen, Piezoresistive properties of cementitious composites reinforced by PVA fibres, *International Conference on Strain-Hardening Cement-Based Composites*, Springer, Dordrecht, September 2017, pp. 709–717.
- [106] M. Luković, D.A. Hordijk, Z. Huang, E. Schlangen, Strain Hardening Cementitious Composite (SHCC) for crack width control in reinforced concrete beams, *Heron* 64 (1/2) (2019) 181.
- [109] M. Xia, B. Nematollahi, J. Sanjayan, Printability, accuracy and strength of geopolymer made using powder-based 3D printing for construction applications, *Autom. Constr.* 101 (2019) 179–189, <https://doi.org/10.1016/j.autcon.2019.01.013>.
- [110] B. Panda, C. Unluer, M.J. Tan, Investigation of the rheology and strength of geopolymer mixtures for extrusion-based 3D printing, *Cem. Concr. Compos.* 94 (2018) 307–314, <https://doi.org/10.1016/j.cemconcomp.2018.10.002>.
- [111] J.H. Lim, B. Panda, Q.C. Pham, Improving flexural characteristics of 3D printed geopolymer composites with in-process steel cable reinforcement, *Constr. Build. Mater.* 178 (2018) 32–41, <https://doi.org/10.1016/j.conbuildmat.2018.05.010>.
- [115] X. Huang, R. Ranade, W. Ni, V.C. Li, Development of green engineered cementitious composites using iron ore tailings as aggregates, *J. Construction and Building Materials* 44 (2013) 757–764.
- [116] M.D. Lepech, V.C. Li, R.E. Robertson, G.A. Keoleian, Design of green engineered cementitious composites for improved sustainability, *ACI Materials J* 105 (6) (2008) 567–575.
- [117] E.H. Yang, Y. Yang, V.C. Li, Use of high volumes of fly ash to improve ECC mechanical properties and material greenness, *ACI Materials J* 104 (6) (2007) 620–628.
- [118] N. Roussel, J. Spangenberg, J. Wallevik, R. Wolfs, Numerical simulations of concrete processing: from standard formative casting to additive manufacturing, *Cement & Concrete Research* (2020), <https://doi.org/10.1016/j.cemconres.2020.106075> (special issue Digital Concrete 2020 (this issue), accepted for publication).
- [119] R. Comminal, M.P. Serdeczny, D.B. Pedersen, J. Spangenberg, Numerical modeling of the strand deposition flow in extrusion-based additive manufacturing, *Additive Manufacturing* 20 (2018) 68–76.
- [120] L. Ferrara, M. Cremonesi, M. Faifer, S. Toscani, L. Sorelli, M.-A. Baril, J. Réthoré, F. Baby, F. Toutlemonde, S. Bernardi, Structural elements made with highly flowable UHPFRC: correlating computational fluid dynamics (CFD) predictions and non-destructive survey of fiber dispersion with failure modes, *Eng. Struct.* 133 (2017) 151–171, <https://doi.org/10.1016/j.engstruct.2016.12.026>.
- [121] R. Lorenzoni, I. Curosu, S. Paciornik, V. Mechtcherine, M. Oppermann, F. Silva, Semantic segmentation of the micro-structure of strain-hardening cement-based composites (SHCC) by applying deep learning on micro-computed tomography scans, *Cem. Concr. Compos.* 108 (May 2019) (2020) 103551, <https://doi.org/10.1016/j.cemconcomp.2020.103551>.
- [122] E. Bosco, R.J.M.A. Claessens, A.S.J. Suiker, Multi-scale prediction of chemo-mechanical properties of concrete materials through asymptotic homogenization, *Cem. Concr. Res.* 128 (October 2019) (2020) 105929, <https://doi.org/10.1016/j.cemconres.2019.105929>.
- [123] S. Qian, M. Lepech, Y.Y. Kim, V.C. Li, Introduction of transition zone design for bridge deck link slabs using ductile concrete, *ACI Structural J* 106 (1) (2009) 96–105.
- [124] T. Kanda, S. Tomoe, K. Miyamoto, Experimental investigation for fire safety of full scale ECC coupling beam, in: V. Mechtcherine, V. Slowik, P. Kabele (Eds.), *Strain-Hardening Cement-Based Composites*, RILEM, 2018, pp. 718–724.
- [125] M. Lepech, V.C. Li, Preliminary findings on size effect in ECC structural members in flexure, in: A.M. Brandt, V.C. Li, I.H. Marshall (Eds.), *Proc., BMC-7, Warsaw, Poland, 2003*, pp. 57–66.
- [126] F. Bos, R. Wolfs, Z. Ahmed, T. Salet, Large scale testing of digitally fabricated concrete (DFC) elements, in: T. Wangler, R. Flatt (Eds.), *First RILEM International Conference on Concrete and Digital Fabrication – Digital Concrete 2018*, DC 2018, RILEM Bookseries, 19 Springer, Cham, 2019, https://doi.org/10.1007/978-3-319-99519-9_12.
- [127] V. Mechtcherine, A. Gram, K. Krenzer, J.-H. Schwabe, S. Shyshko, N. Roussel, Simulation of fresh concrete flow using Discrete Element Method (DEM): theory and applications, *Mater. Struct.* 47 (4) (2014) 615–630.